PHYSICAL REVIEW D **78,** 074007 (2008)

$K_1(1270) - K_1(1400)$ mixing angle and new-physics effects in $B \to K_1 l^+ l^-$ decays

Hisaki Hatanaka and Kwei-Chou Yang

Department of Physics, Chung-Yuan Christian University, Chungli 320, Taiwan

(Received 28 August 2008; published 7 October 2008)

We study semileptonic B meson decays $B \to K_1(1270)\ell^+\ell^-$ and $K_1(1400)\ell^+\ell^-$ ($\ell \equiv e, \mu, \tau$), where the strange P-wave mesons, $K_1(1270)$ and $K_1(1400)$, are the mixtures of the K_{1A} and K_{1B}, which are the 1^3P_1 and 1^1P_1 states, respectively. We show that the ratio $R_\ell \equiv \mathcal{B}(B \to K_1(1400)\ell^+\ell^-)/\mathcal{B}(B \to K_1(1270)\ell^+\ell^-)$, insensitive to new-physics parameters, is suitable for determining the $K_1(1270) - K_1(1400)$ mixing angle, θ_{K_1}. The forward-backward asymmetry shows a weak θ_{K_1} dependence for $B \to K_1(1270)\mu^+\mu^-$, but relatively strong for $B \to K_1(1400)\mu^+\mu^-$. We investigate model-independent new-physics corrections to operators relevant to the $b \to s\ell^+\ell^-$ electroweak-penguin and weak-box diagrams. Furthermore, for the $B \to K_1(1270)\mu^+\mu^-$ decay the position of the forward-backward asymmetry zero, which is almost independent of the value of θ_{K_1}, can be dramatically changed under variation of new-physics parameters.

DOI: 10.1103/PhysRevD.78.074007 PACS numbers: 13.20.He, 12.60.−i, 14.40.Ev

I. INTRODUCTION

$b \to s$ transitions in semileptonic and radiative B meson decays contain rich phenomena relevant to the standard model (SM) and new physics (NP). Semileptonic and radiative B decays involving a vector or axial-vector meson have been observed by *BABAR*, Belle, and CLEO (see Table I). The rare flavor-changing neutral-current processes, $b \to s\bar{\ell}\ell$, which proceed through the electroweak-penguin and weak-box diagrams in the SM, may provide a hunting ground to search for the NP effects. For $B \to K^*(892)\ell^+\ell^-$ decays, the forward-backward asymmetry has been measured by *BABAR* [7] and Belle [8]. Very recently, *BABAR* [9–11] has reported the measurements for the longitudinal polarization fraction and forward-backward asymmetry (FBA) of $B \to K^*(892)\ell^+\ell^-$, and for the isospin asymmetry of $B^0 \to K^{*0}(892)\ell^+\ell^-$ and $B^\pm \to K^{*\pm}(892)\ell^+\ell^-$ channels. The data may hint at the flipped sign(s) of the Wilson coefficients, e.g., the flipped sign of $c_7^{\rm eff}$ related to the magnetic dipole operator. To extract the moduli and arguments of the effective Wilson coefficients, it is important to measure various observables in different inclusive and exclusive rare processes. These should be considerably improved at LHCb.

The radiative B decay involving the $K_1(1270)$, the orbitally excited (P-wave) state, was recently observed by Belle and other radiative and semileptonic decay modes involving $K_1(1270)$ and $K_1(1400)$ are hopefully expected to be seen soon. Some studies for $B \to K_1\ell^+\ell^-$ have been made recently [12–14]. Just like $B \to K^*(892)\ell^+\ell^-$ decays [15–22], $B \to K_1\ell^+\ell^-$ decays can offer the good probe to the NP, and are much more sophisticated due to the mixing of the K_{1A} and K_{1B}, which are the 1^3P_1 and 1^1P_1 states, respectively. The physical K_1 mesons are $K_1(1270)$ and $K_1(1400)$, described by

$$\begin{pmatrix} |\bar{K}_1(1270)\rangle \\ |\bar{K}_1(1400)\rangle \end{pmatrix} = M \begin{pmatrix} |\bar{K}_{1A}\rangle \\ |\bar{K}_{1B}\rangle \end{pmatrix}, \quad \text{with } M = \begin{pmatrix} \sin\theta_{K_1} & \cos\theta_{K_1} \\ \cos\theta_{K_1} & -\sin\theta_{K_1} \end{pmatrix}. \tag{1}$$

The magnitude of θ_{K_1} was estimated to be $|\theta_{K_1}| \approx 34^\circ \vee 57^\circ$ in Ref. [23], $35^\circ \lesssim |\theta_{K_1}| \lesssim 55^\circ$ in Ref. [24], and $|\theta_{K_1}| = 37^\circ \vee 58^\circ$ in Ref. [25]. Nevertheless, the sign of the θ_{K_1} was not yet determined in these studies. From the study for $B \to K_1(1270)\gamma$ and $\tau \to K_1(1270)\nu_\tau$, we recently obtain [26]

$$\theta_{K_1} = -(34 \pm 13)^\circ, \tag{2}$$

where the minus sign of θ_{K_1} is related to the chosen phase of $|\bar{K}_{1A}\rangle$ and $|\bar{K}_{1B}\rangle$. We adopt the following conventions [26]: $f_{K_{1A}} > 0$ and $f^\perp_{K_{1B}} > 0$, which are defined by

$$\begin{aligned} \langle 0|\bar{\psi}\gamma^\mu\gamma_5 s|\bar{K}_{1A}(P,\lambda)\rangle &= -if_{K_{1A}} m_{K_{1A}} \varepsilon_\mu^{(\lambda)}, \\ \langle 0|\bar{\psi}\sigma_{\mu\nu} s|\bar{K}_{1B}(P,\lambda)\rangle &= if^\perp_{K_{1B}} \epsilon_{\mu\nu\alpha\beta}\varepsilon^\alpha_{(\lambda)} P^\beta, \\ \psi &\equiv d, u. \end{aligned} \tag{3}$$

Within the SM, we have predicted [26]

$$\mathcal{B}(B^- \to K_1^-(1270)\gamma) = (66^{+50}_{-30}) \times 10^{-6}\left(\frac{m_{b,\rm pole}}{4.90\ \rm GeV}\right)^2, \tag{4}$$

$$\mathcal{B}(B^- \to K_1^-(1400)\gamma) = (6.5^{+12.8}_{-6.3}) \times 10^{-6}\left(\frac{m_{b,\rm pole}}{4.90\ \rm GeV}\right)^2, \tag{5}$$

where $m_{b,\rm pole}$ is the pole mass of the b quark. In the present paper, we study the observables for $B \to K_1\ell^+\ell^-$ decays, including the dilepton mass spectra, decay rates, and

 © 2008 The American Physical Society

TABLE I. Experimental status of branching fractions (in units of 10^{-6}) for the decays $B \to K^*(892)\gamma$, $K_1(1270)\gamma$, $K_1(1400)\gamma$, and $B \to K^*(892)\ell^+\ell^-$ [1].

Mode	Exp.(Average)	Ref.	Mode	Exp.(Average)	Ref.
$K^{*+}(892)\gamma$	40.3 ± 2.6	[2–4]	$K^{*0}(892)\gamma$	40.1 ± 2.0	[2–4]
$K_1^+(1270)\gamma$	43 ± 12	[5]	$K_1^0(1270)\gamma$	<58	[5]
$K_1^+(1400)\gamma$	<15	[5]	$K_1^0(1400)\gamma$	<15	[5]
$K^{*+}(892)e^+e^-$	$1.23^{+0.69}_{-0.62}$	[6,7]	$K^{*0}(892)e^+e^-$	$1.11^{+0.30}_{-0.26}$	[6,7]
$K^{*+}(892)\mu^+\mu^-$	$0.78^{+0.56}_{-0.44}$	[6,7]	$K^{*0}(892)\mu^+\mu^-$	$0.98^{+0.22}_{-0.21}$	[6,7]

forward-backward asymmetries. We further show that the mixing angle θ_{K_1} can be determined from the $B \to K_1\ell^+\ell^-$ decays. In addition to the study of the θ_{K_1}, we also investigate the model-independent new-physics corrections to the Wilson coefficients $c_7^{\rm eff}$, c_9, and c_{10}. The new-physics parameters can be well constrained by the measurement of $B \to K_1\ell^+\ell^-$ FBA, where the position of the FBA zero depends very weakly on the value of the θ_{K_1}. Hence, the position of zero of the differential FBAs depends on the underlying new-physics corrections.

This paper is organized as follows. In Sec. II, we introduce the effective Hamiltonian and effective operators therein. In Sec. III, we give the definitions for $B \to K_1(1270)$ and $B \to K_1(1400)$ form factors. In Sec. IV, we formulate the $B \to K_1\ell^+\ell^-$ decays and discuss determination of the θ_{K_1} in details. In Sec. V, we estimate the NP effects in the model-independent way. We summarize the main results in Sec. VI.

II. THE EFFECTIVE HAMILTONIAN

Neglecting doubly Cabibbo-suppressed contributions, the effective weak Hamiltonian relevant to $b \to s\ell^+\ell^-$ is given by

$$\mathcal{H}_{\rm eff} = -4\frac{G_F}{\sqrt{2}}V_{tb}V_{ts}^*\sum_{i=1}^{10}c_i(\mu)O_i(\mu), \tag{6}$$

where the Wilson operators O_i for $i = 1, \cdots, 10$ read [27]

$$O_1 = (\bar{s}_\alpha\gamma_\mu Lc_\alpha)(\bar{c}_\beta\gamma^\mu Lb_\beta), \quad O_2 = (\bar{s}_\alpha\gamma_\mu Lc_\beta)(\bar{c}_\beta\gamma^\mu Lb_\alpha), \quad O_3 = (\bar{s}_\alpha\gamma_\mu Lb_\alpha)\sum_q(\bar{q}_\beta\gamma^\mu Lq_\beta),$$
$$O_4 = (\bar{s}_\alpha\gamma_\mu Lb_\beta)\sum_q(\bar{q}_\beta\gamma^\mu Lq_\alpha), \quad O_5 = (\bar{s}_\alpha\gamma_\mu Lb_\alpha)\sum_q(\bar{q}_\beta\gamma^\mu Rq_\beta), \quad O_6 = (\bar{s}_\alpha\gamma_\mu Lb_\beta)\sum_q(\bar{q}_\beta\gamma^\mu Rq_\alpha),$$
$$O_7 = \frac{em_b}{16\pi^2}\bar{s}\sigma^{\mu\nu}RbF_{\mu\nu}, \quad O_9 = \frac{\alpha_{\rm em}}{4\pi}(\bar{\ell}\gamma_\mu\ell)(\bar{s}\gamma^\mu Lb), \quad O_{10} = \frac{\alpha_{\rm em}}{4\pi}(\bar{\ell}\gamma_\mu\gamma_5\ell)(\bar{s}\gamma^\mu Lb), \tag{7}$$

with $L = (1-\gamma_5)/2$, $R = (1+\gamma_5)/2$, and α, β being the $SU(3)$ color indices. The $b \to s\ell^+\ell^-$ decay amplitude is given by

$$\mathcal{M}(b \to s\ell^+\ell^-) = \frac{G_F}{\sqrt{2}}\frac{\alpha_{\rm em}}{\pi}V_{ts}^*V_{tb}\Big\{c_9^{\rm eff}(\hat{s})[\bar{s}\gamma_\mu Lb][\bar{\ell}\gamma^\mu\ell] + c_{10}[\bar{s}\gamma_\mu Lb][\bar{\ell}\gamma^\mu\ell] - 2\hat{m}_b c_7^{\rm eff}\Big[\bar{s}i\sigma_{\mu\nu}\frac{\hat{q}^\nu}{\hat{s}}Rb\Big][\bar{\ell}\gamma^\mu\ell]\Big\}, \tag{8}$$

where $\hat{m}_b \equiv \bar{m}_b/m_B$ with $\bar{m}_b = \bar{m}_b(\bar{m}_b)$ being the b quark mass in the $\overline{\rm MS}$ scheme, $\hat{s} = q^2/m_B^2$, $q_\mu = (p_+ + p_-)_\mu$ with $p_\pm$ being momenta of the leptons $\ell^\pm$. To next-to-leading order the running $\overline{\rm MS}$ and pole b-quark masses are related by

$$\bar{m}_b(\mu) = m_{b,\rm pole}\Big[1 - \frac{\alpha_s(\mu)C_F}{4\pi}\Big(4 - 3\ln\frac{m_{b,\rm pole}^2}{\mu^2}\Big) + \mathcal{O}(\alpha_s^2)\Big], \tag{9}$$

where $C_F = (N_c^2-1)/(2N_c)$ with N_c being the number of colors. In Eq. (8) we have neglected $\mathcal{O}(m_s/m_b)$ corrections. $c_9^{\rm eff}(\hat{s}) = c_9 + Y(\hat{s})$, where $Y(\hat{s}) = Y_{\rm pert}(\hat{s}) + Y_{\rm LD}$ contains both the perturbative part $Y_{\rm pert}(\hat{s})$ and long-distance part $Y_{\rm LD}(\hat{s})$. $Y(\hat{s})_{\rm pert}$ is given by [28]

$$Y_{\rm pert}(\hat{s}) = g(\hat{m}_c, \hat{s})c_0 - \tfrac{1}{2}g(1, \hat{s})(4\bar{c}_3 + 4\bar{c}_4 + 3\bar{c}_5 + \bar{c}_6) - \tfrac{1}{2}g(0, \hat{s})(\bar{c}_3 + 3\bar{c}_4) + \tfrac{2}{9}(3\bar{c}_3 + \bar{c}_4 + 3\bar{c}_5 + \bar{c}_6), \tag{10}$$

with

$$c_0 \equiv \bar{c}_1 + 3\bar{c}_2 + 3\bar{c}_3 + \bar{c}_4 + 3\bar{c}_5 + \bar{c}_6, \tag{11}$$

and the function $g(x, y)$ defined in [28]. Here $\bar{c}_1$–$\bar{c}_6$ are the Wilson coefficients in the leading logarithmic approximation. The relevant Wilson coefficients are collected in Table II [15,27]. $Y(\hat{s})_{\rm LD}$ involves $B \to K_1V(\bar{c}c)$ resonances [29–31], where $V(\bar{c}c)$ are the vector charmonium states. We follow Refs. [29,30] and set

TABLE II. The Wilson coefficients $c_i(\mu)$ at the scale $\mu = m_{b,\mathrm{pole}}$ in the SM. Here $c_7^{\mathrm{eff}} \equiv c_7 - \frac{1}{3}c_5 - c_6$.

$\bar{c}_1$	$\bar{c}_2$	$\bar{c}_3$	$\bar{c}_4$	$\bar{c}_5$	$\bar{c}_6$	c_7^{eff}	c_9	c_{10}
+1.107	−0.248	−0.011	−0.026	−0.007	−0.031	−0.313	4.344	−4.669

TABLE III. Masses, total decay widths, and branching fractions of dilepton decays of vector charmonium states [32].

V	Mass [GeV]	Γ_{tot}^V [MeV]	$\mathcal{B}(V \to \ell^+\ell^-)$	
$J/\Psi(1S)$	3.097	0.093	5.9×10^{-2}	for $\ell = e, \mu$
$\Psi(2S)$	3.686	0.327	7.4×10^{-3}	for $\ell = e, \mu$
			3.0×10^{-3}	for $\ell = \tau$
$\Psi(3770)$	3.772	25.2	9.8×10^{-6}	for $\ell = e$
$\Psi(4040)$	4.040	80	1.1×10^{-5}	for $\ell = e$
$\Psi(4160)$	4.153	103	8.1×10^{-6}	for $\ell = e$
$\Psi(4415)$	4.421	62	9.4×10^{-6}	for $\ell = e$

$$Y_{\mathrm{LD}}(\hat{s}) = -\frac{3\pi}{\alpha_{\mathrm{em}}^2} c_0 \sum_{V=\psi(1s),\cdots} \kappa_V \frac{\hat{m}_V \mathcal{B}(V \to \ell^+\ell^-)\hat{\Gamma}_{\mathrm{tot}}^V}{\hat{s} - \hat{m}_V^2 + i\hat{m}_V\hat{\Gamma}_{\mathrm{tot}}^V}, \tag{12}$$

where $\hat{\Gamma}_{\mathrm{tot}}^V \equiv \Gamma_{\mathrm{tot}}^V/m_B$ and $\kappa_V = 2.3$. The relevant properties of vector charmonium states are summarized in Table III.

III. $B \to K_1(1270)$ AND $B \to K_1(1400)$ FORM FACTORS

The $\bar{B}(p_B) \to \bar{K}_1(p_{K_1}, \lambda)$ form factors are defined by

$$\begin{aligned} &\langle \bar{K}_1(p_{K_1}, \lambda)|\bar{\psi}\gamma_\mu(1-\gamma_5)b|\bar{B}(p_B)\rangle \\ &= -i\frac{2}{m_B + m_{K_1}} \epsilon_{\mu\nu\rho\sigma}\varepsilon_{(\lambda)}^{*\nu} p_B^\rho p_{K_1}^\sigma A^{K_1}(q^2) \\ &\quad - \Big[(m_B + m_{K_1})\varepsilon_\mu^{(\lambda)*} V_1^{K_1}(q^2) \\ &\quad - (p_B + p_{K_1})_\mu (\varepsilon_{(\lambda)}^* \cdot p_B)\frac{V_2^{K_1}(q^2)}{m_B + m_{K_1}}\Big] \\ &\quad + 2m_{K_1}\frac{\varepsilon_{(\lambda)}^* \cdot p_B}{q^2} q_\mu [V_3^{K_1}(q^2) - V_0^{K_1}(q^2)], \end{aligned} \tag{13}$$

$$\begin{aligned} &\langle \bar{K}_1(p_{K_1}, \lambda)|\bar{\psi}\sigma_{\mu\nu}q^\nu(1+\gamma_5)b|\bar{B}(p_B)\rangle \\ &= 2T_1^{K_1}(q^2)\epsilon_{\mu\nu\rho\sigma}\varepsilon_{(\lambda)}^{*\nu} p_B^\rho p_{K_1}^\sigma - iT_2^{K_1}(q^2) \\ &\quad \times [(m_B^2 - m_{K_1}^2)\varepsilon_{*\mu}^{(\lambda)} - (\varepsilon_{(\lambda)}^* \cdot q)(p_B + p_{K_1})_\mu] \\ &\quad - iT_3^{K_1}(q^2)(\varepsilon_{(\lambda)}^* \cdot q)\Big[q_\mu - \frac{q^2}{m_B^2 - m_{K_1}^2}(p_{K_1} + p_B)_\mu\Big], \end{aligned} \tag{14}$$

where $q \equiv p_B - p_{K_1}$, $\gamma_5 \equiv i\gamma^0\gamma^1\gamma^2\gamma^3$, $\epsilon^{0123} = -1$, and $\psi \equiv d, s$. The form factors satisfy the following relations,

$$\begin{aligned} &V_3^{K_1}(0) = V_0^{K_1}(0), \qquad T_1^{K_1}(0) = T_2^{K_1}(0), \\ &V_3^{K_1}(q^2) = \frac{m_B + m_{K_1}}{2m_{K_1}} V_1^{K_1}(q^2) - \frac{m_B - m_{K_1}}{2m_{K_1}} V_2^{K_1}(q^2). \end{aligned} \tag{15}$$

Because the $K_1(1270)$ and $K_1(1400)$ are the mixing states of the K_{1A} and K_{1B}, the $\bar{B} \to \bar{K}_1$ form factors can be parametrized by

$$\begin{pmatrix} \langle \bar{K}_1(1270)|\bar{s}\gamma_\mu(1-\gamma_5)b|\bar{B}\rangle \\ \langle \bar{K}_1(1400)|\bar{s}\gamma_\mu(1-\gamma_5)b|\bar{B}\rangle \end{pmatrix} = M\begin{pmatrix} \langle \bar{K}_{1A}|\bar{s}\gamma_\mu(1-\gamma_5)b|\bar{B}\rangle \\ \langle \bar{K}_{1B}|\bar{s}\gamma_\mu(1-\gamma_5)b|\bar{B}\rangle \end{pmatrix}, \tag{16}$$

$$\begin{pmatrix} \langle \bar{K}_1(1270)|\bar{s}\sigma_{\mu\nu}q^\nu(1+\gamma_5)b|\bar{B}\rangle \\ \langle \bar{K}_1(1400)|\bar{s}\sigma_{\mu\nu}q^\nu(1+\gamma_5)b|\bar{B}\rangle \end{pmatrix} = M\begin{pmatrix} \langle \bar{K}_{1A}|\bar{s}\sigma_{\mu\nu}q^\nu(1+\gamma_5)b|\bar{B}\rangle \\ \langle \bar{K}_{1B}|\bar{s}\gamma_{\mu\nu}q^\nu(1+\gamma_5)b|\bar{B}\rangle \end{pmatrix}, \tag{17}$$

with the mixing matrix M being given in Eq. (1). Thus the form factors A^{K_1}, $V_{0,1,2}^{K_1}$,and $T_{1,2,3}^{K_1}$ satisfy the following relations:

$$\begin{pmatrix} A^{K_1(1270)}/(m_B + m_{K_1(1270)}) \\ A^{K_1(1400)}/(m_B + m_{K_1(1400)}) \end{pmatrix} = M\begin{pmatrix} A^{K_{1A}}/(m_B + m_{K_{1A}}) \\ A^{K_{1B}}/(m_B + m_{K_{1B}}) \end{pmatrix}, \tag{18}$$

$$\begin{pmatrix} (m_B + m_{K_1(1270)})V_1^{K_1(1270)} \\ (m_B + m_{K_1(1400)})V_1^{K_1(1400)} \end{pmatrix} = M\begin{pmatrix} (m_B + m_{K_{1A}})V_1^{K_{1A}} \\ (m_B + m_{K_{1B}})V_1^{K_{1B}} \end{pmatrix}, \tag{19}$$

TABLE IV. Form factors for $B \to K_{1A}, K_{1B}$ transitions obtained in the light-cone sum rule calculation [33,34] are fitted to the three-parameter form in Eq. (25).

F	$F(0)$	a	b	F	$F(0)$	a	b
$V_1^{BK_{1A}}$	0.34 ± 0.07	0.635	0.211	$V_1^{BK_{1B}}$	$-0.29^{+0.08}_{-0.05}$	0.729	0.074
$V_2^{BK_{1A}}$	0.41 ± 0.08	1.51	1.18	$V_2^{BK_{1B}}$	$-0.17^{+0.05}_{-0.03}$	0.919	0.855
$V_0^{BK_{1A}}$	0.22 ± 0.04	2.40	1.78	$V_0^{BK_{1B}}$	$-0.45^{+0.12}_{-0.08}$	1.34	0.690
$A^{BK_{1A}}$	0.45 ± 0.09	1.60	0.974	$A^{BK_{1B}}$	$-0.37^{+0.10}_{-0.06}$	1.72	0.912
$T_1^{BK_{1A}}$	$0.31^{+0.09}_{-0.05}$	2.01	1.50	$T_1^{BK_{1B}}$	$-0.25^{+0.06}_{-0.07}$	1.59	0.790
$T_2^{BK_{1A}}$	$0.31^{+0.09}_{-0.05}$	0.629	0.387	$T_2^{BK_{1B}}$	$-0.25^{+0.06}_{-0.07}$	0.378	−0.755
$T_3^{BK_{1A}}$	$0.28^{+0.08}_{-0.05}$	1.36	0.720	$T_3^{BK_{1B}}$	-0.11 ± 0.02	−1.61	10.2

$$\begin{pmatrix} V_2^{K_1(1270)}/(m_B + m_{K_1(1270)}) \\ V_2^{K_1(1400)}/(m_B + m_{K_1(1400)}) \end{pmatrix} = M \begin{pmatrix} V_2^{K_{1A}}/(m_B + m_{K_{1A}}) \\ V_2^{K_{1B}}/(m_B + m_{K_{1B}}) \end{pmatrix}, \tag{20}$$

$$\begin{pmatrix} m_{K_1(1270)} V_0^{K_1(1270)} \\ m_{K_1(1400)} V_0^{K_1(1400)} \end{pmatrix} = M \begin{pmatrix} m_{K_{1A}} V_0^{K_{1A}} \\ m_{K_{1B}} V_0^{K_{1B}} \end{pmatrix}, \tag{21}$$

$$\begin{pmatrix} T_1^{K_1(1270)} \\ T_1^{K_1(1400)} \end{pmatrix} = M \begin{pmatrix} T_1^{K_{1A}} \\ T_1^{K_{1B}} \end{pmatrix}, \tag{22}$$

$$\begin{pmatrix} (m_B^2 - m_{K_1(1270)}^2) T_2^{K_1(1270)} \\ (m_B^2 - m_{K_1(1400)}^2) T_2^{K_1(1400)} \end{pmatrix} = M \begin{pmatrix} (m_B^2 - m_{K_{1A}}^2) T_2^{K_{1A}} \\ (m_B^2 - m_{K_{1B}}^2) T_2^{K_{1B}} \end{pmatrix}, \tag{23}$$

$$\begin{pmatrix} T_3^{K_1(1270)} \\ T_3^{K_1(1400)} \end{pmatrix} = M \begin{pmatrix} T_3^{K_{1A}} \\ T_3^{K_{1B}} \end{pmatrix}, \tag{24}$$

where we have assumed that $p^\mu_{K_1(1270),K_1(1400)} \simeq p^\mu_{K_{1A}} \simeq p^\mu_{K_{1B}}$. For the numerical analysis, we use the light-cone sum rule results for the form factors [33,34] which are exhibited in Table IV, where the momentum dependence is parametrized in the three-parameter form,

$$F(q^2) = \frac{F(0)}{1 - a(q^2/m_B^2) + b(q^2/m_B^2)^2}. \tag{25}$$

IV. $\bar{B} \to \bar{K}_1 \ell^+ \ell^-$ DECAYS IN THE SM

The decay amplitude for $B \to K_1 \ell^+ \ell^-$ which is analogous to the $B \to K^*(892)\ell^+\ell^-$ decay [15] is given by

$$\mathcal{M} = \frac{G_F \alpha_{\rm em}}{2\sqrt{2}\pi} V_{ts}^* V_{tb} m_B \cdot (-i)[\mathcal{T}_\mu^{(K_1),1} \bar{\ell}\gamma^\mu \ell + \mathcal{T}_\mu^{(K_1),2} \bar{\ell}\gamma^\mu \gamma_5 \ell], \tag{26}$$

where

$$\mathcal{T}_\mu^{(K_1),1} = \mathcal{A}^{K_1}(\hat{s})\epsilon_{\mu\nu\rho\sigma}\varepsilon^{*\nu}\hat{p}_B^\rho \hat{p}_{K_1}^\sigma - i\mathcal{B}^{K_1}(\hat{s})\varepsilon^*_\mu + i\mathcal{C}^{K_1}(\hat{s})(\varepsilon^* \cdot \hat{p}_B)\hat{p}_\mu + i\mathcal{D}^{K_1}(\hat{s})(\varepsilon^* \cdot \hat{p}_B)\hat{q}_\mu, \tag{27}$$

$$\mathcal{T}_\mu^{(K_1),2} = \mathcal{E}^{K_1}(\hat{s})\epsilon_{\mu\nu\rho\sigma}\varepsilon^{*\nu}\hat{p}_B^\rho \hat{p}_{K_1}^\sigma - i\mathcal{F}^{K_1}(\hat{s})\varepsilon^*_\mu + i\mathcal{G}^{K_1}(\hat{s}) \times (\varepsilon^* \cdot \hat{p}_B)\hat{p}_\mu + i\mathcal{H}^{K_1}(\hat{s})(\varepsilon^* \cdot \hat{p}_B)\hat{q}_\mu, \tag{28}$$

with $\hat{p} = p/m_B$, $\hat{p}_B = p_B/m_B$, $\hat{q} = q/m_B$ and $p = p_B + p_{K_1}$, $q = p_B - p_{K_1} = p_+ + p_-$. Here $\mathcal{A}^{K_1}(\hat{s}), \cdots, \mathcal{H}^{K_1}(\hat{s})$ are defined by

$$\mathcal{A}^{K_1}(\hat{s}) = \frac{2}{1 + \hat{m}_{K_1}} c_9^{\rm eff}(\hat{s}) A^{K_1}(\hat{s}) + \frac{4\hat{m}_b}{\hat{s}} c_7^{\rm eff} T_1^{K_1}(\hat{s}), \tag{29}$$

$$\mathcal{B}^{K_1}(\hat{s}) = (1 + \hat{m}_{K_1})\bigg[c_9^{\rm eff}(\hat{s}) V_1^{K_1}(\hat{s}) + \frac{2\hat{m}_b}{\hat{s}}(1 - \hat{m}_{K_1}) c_7^{\rm eff} T_2^{K_1}(\hat{s})\bigg], \tag{30}$$

$$\mathcal{C}^{K_1}(\hat{s}) = \frac{1}{1 - \hat{m}_{K_1}^2}\bigg[(1 - \hat{m}_{K_1}) c_9^{\rm eff}(\hat{s}) V_2^{K_1}(\hat{s}) + 2\hat{m}_b c_7^{\rm eff}\bigg(T_3^{K_1}(\hat{s}) + \frac{1 - \hat{m}_{K_1}^2}{\hat{s}} T_2^{K_1}(\hat{s})\bigg)\bigg], \tag{31}$$

$$\mathcal{D}^{K_1}(\hat{s}) = \frac{1}{\hat{s}}[c_9^{\rm eff}(\hat{s})\{(1 + \hat{m}_{K_1})V_1^{K_1}(\hat{s}) - (1 - \hat{m}_{K_1})V_2^{K_1}(\hat{s}) - 2\hat{m}_{K_1} V_0^{K_1}(\hat{s})\} - 2\hat{m}_b c_7^{\rm eff} T_3^{K_1}(\hat{s})], \tag{32}$$

$$\mathcal{E}^{K_1}(\hat{s}) = \frac{2}{1 + \hat{m}_{K_1}} c_{10} A^{K_1}(\hat{s}), \tag{33}$$

$$\mathcal{F}^{K_1}(\hat{s}) = (1 + \hat{m}_{K_1}) c_{10} V_1^{K_1}(\hat{s}), \tag{34}$$

$$\mathcal{G}^{K_1}(\hat{s}) = \frac{1}{1 + \hat{m}_{K_1}} c_{10} V_2^{K_1}(\hat{s}), \tag{35}$$

$$\mathcal{H}^{K_1}(\hat{s}) = \frac{1}{\hat{s}} c_{10}[(1 + \hat{m}_{K_1})V_1^{K_1}(\hat{s}) - (1 - \hat{m}_{K_1})V_2^{K_1}(\hat{s}) - 2\hat{m}_{K_1} V_0^{K_1}(\hat{s})], \tag{36}$$

with $\hat{m}_{K_1} = m_{K_1}/m_B$. We choose $\hat{s} = \hat{q}^2$ and $\hat{u} \equiv (\hat{p}_B - \hat{p}_-)^2 - (\hat{p}_B - \hat{p}_+)^2$ as the two independent parameters, which are bounded as $4\hat{m}_l^2 \le \hat{s} \le (1 - \hat{m}_{K_1})^2$ and $-\hat{u}(\hat{s}) \le \hat{u} \le \hat{u}(\hat{s})$, with $\hat{u}(\hat{s}) \equiv \sqrt{\lambda(1 - 4\hat{m}_l^2/\hat{s})}$, $\lambda \equiv 1 + \hat{m}_{K_1}^2 + \hat{s}^2 - 2\hat{s} - 2\hat{m}_{K_1}^2(1 + \hat{s})$. We have $\hat{u} = -\hat{u}(\hat{s})\cos\theta$, where θ is the angle between the momenta of ℓ^+ and the b quark in the center-of-mass frame of the lepton pair. We will use the parameters given in Tables IV and V in the numerical analysis.

A. Dilepton mass spectrum

The dilepton invariant mass spectrum of the lepton pair for the $\bar{B} \to \bar{K}_1 \ell^+ \ell^-$ decay is given by

$$\begin{aligned}\frac{d\Gamma(\bar{B} \to \bar{K}_1 \ell^+ \ell^-)}{d\hat{s}} &= \frac{G_F^2 \alpha_{\rm em}^2 m_B^5}{2^{10}\pi^5} |V_{tb}V_{ts}^*|^2 \hat{u}(\hat{s}) \times \bigg\{ \frac{|\mathcal{A}^{K_1}|^2}{3} \hat{s}\lambda\bigg(1 + 2\frac{\hat{m}_\ell^2}{\hat{s}}\bigg) + |\mathcal{E}^{K_1}|^2 \hat{s}\frac{\hat{u}(\hat{s})^2}{3} + \frac{1}{4\hat{m}_{K_1}^2}\bigg[|\mathcal{B}^{K_1}|^2\bigg(\lambda - \frac{\hat{u}(\hat{s})^2}{3} \\ &\quad + 8\hat{m}_{K_1}^2(\hat{s} + 2\hat{m}_\ell^2)\bigg) + |\mathcal{F}^{K_1}|^2\bigg(\lambda - \frac{\hat{u}(\hat{s})^2}{3} + 8\hat{m}_{K_1}^2(\hat{s} - 4\hat{m}_\ell^2)\bigg)\bigg] + \frac{\lambda}{4\hat{m}_{K_1}^2}\bigg[|\mathcal{C}^{K_1}|^2\bigg(\lambda - \frac{\hat{u}(\hat{s})^2}{3}\bigg) \\ &\quad + |\mathcal{G}^{K_1}|^2\bigg(\lambda - \frac{\hat{u}(\hat{s})^2}{3} + 4\hat{m}_\ell^2(2 + 2\hat{m}_{K_1}^2 - \hat{s})\bigg)\bigg] - \frac{1}{2\hat{m}_{K_1}^2}\bigg[{\rm Re}(\mathcal{B}^{K_1}\mathcal{C}^{K_1 *})\bigg(\lambda - \frac{\hat{u}(\hat{s})^2}{3}\bigg)(1 - \hat{m}_{K_1}^2 - \hat{s}) \\ &\quad + {\rm Re}(\mathcal{F}^{K_1}\mathcal{G}^{K_1 *})\bigg(\bigg(\lambda - \frac{\hat{u}(\hat{s})^2}{3}\bigg)(1 - \hat{m}_{K_1}^2 - \hat{s}) + 4\hat{m}_\ell^2\lambda\bigg)\bigg] - 2\frac{\hat{m}_\ell^2}{\hat{m}_{K_1}^2}\lambda[{\rm Re}(\mathcal{F}^{K_1}\mathcal{H}^{K_1 *}) - {\rm Re}(\mathcal{G}^{K_1}\mathcal{H}^{K_1 *}) \\ &\quad \times (1 - \hat{m}_{K_1}^2)] + \frac{\hat{m}_\ell^2}{\hat{m}_{K_1}^2}\hat{s}\lambda|\mathcal{H}^{K_1}|^2\bigg\}. \end{aligned} \tag{37}$$

The differential decay rates $d\mathcal{B}(B^- \to K_1^- \mu^+ \mu^-)/ds \equiv \tau_{B^-} \times d\Gamma(B \to K_1^- \mu^+ \mu^-)/ds$ are plotted in Fig. 1. To illustrate the dependence on θ_{K_1}, we plot the distributions for the differential decay rates with $\theta_{K_1} = -34°$, $-45°$, and $-57°$, respectively. The effects of charmonium resonances become large for the large region with $s \gtrsim 5\ \text{GeV}^2$. We find that in the low s region, where $s \approx 2\ \text{GeV}^2$, the differential decay rate for $B \to K_1(1400)\mu^+\mu^-$ with $\theta_{K_1} = -57°$ is enhanced by about 80% compared with $\theta_{K_1} = -34°$, whereas the rates for $B \to K_1(1270)\mu^+\mu^-$ are not so sensitive to the variation of θ_{K_1}. One should note that the distribution in the low s region is dominated by the $1/s$ term arising from $B \to K_1\gamma$; for instance, for the $B \to K_1(1270)\mu^+\mu^-$ decay, it results in the peak at $s \sim 4m_\ell^2$ (or exactly at $s = 0$) and contributes about -30% at around $s = 2\ \text{GeV}^2$ for $-57° < \theta_{K_1} < -34°$.

Furthermore, the value of θ_{K_1} can be well determined from the following ratio of the distributions,

$$R_{d\Gamma/ds,\mu} \equiv \frac{d\Gamma(B^- \to K_1^-(1400)\mu^+\mu^-)/ds}{d\Gamma(B^- \to K_1^-(1270)\mu^+\mu^-)/ds}. \tag{38}$$

In Fig. 2, we plot the $R_{d\Gamma/ds,\mu}$ as a function of s, which is highly insensitive to the resonance contributions and form

TABLE V. Input parameters.

B meson mass and lifetimes [32]
$m_B = 5.279$ GeV, $\tau_{B^-} = 1.638 \times 10^{-12}$ sec, $\tau_{B^0} = 1.530 \times 10^{-12}$ sec
Axial-vector meson masses [GeV]
$m_{K_1(1270)} = 1.272$ [32], $m_{K_1(1400)} = 1.403$ [32], $m_{K_{1A}} = 1.31$ [35], $m_{K_{1B}} = 1.34$ [35]
CKM matrix elements
$\lvert V_{tb}V_{ts}^*\rvert = 0.0407^{+0.0009}_{-0.0008}$ [36]
b quark mass [GeV]
$m_{b,\rm pole} = 4.8 \pm 0.2$
Gauge couplings and the parameter for the B meson distribution amplitude
$\alpha_{\rm em} = 1/129$, $\alpha_s(\mu_h) = 0.3$, $\lambda_{B,+}^{-1} = 3 \pm 1\ \text{GeV}^{-1}$ [16]
K_1 decay constants [MeV] [35]
$f_{K_{1A}}^{\parallel} = 250 \pm 13$, $f_{K_{1B}}^{\perp}[1\ \text{GeV}] = 190 \pm 10$
Gegenbauer moments at the scale 2.2 GeV [35]
$a_0^{K_{1A},\perp} = 0.24^{+0.03}_{-0.21}$, $a_1^{K_{1A},\perp} = -0.84 \pm 0.37$, $a_2^{K_{1A},\perp} = 0.01 \pm 0.15$,
$a_1^{K_{1B},\perp} = 0.25^{+0.00}_{-0.26}$, $a_2^{K_{1B},\perp} = -0.02 \pm 0.17$

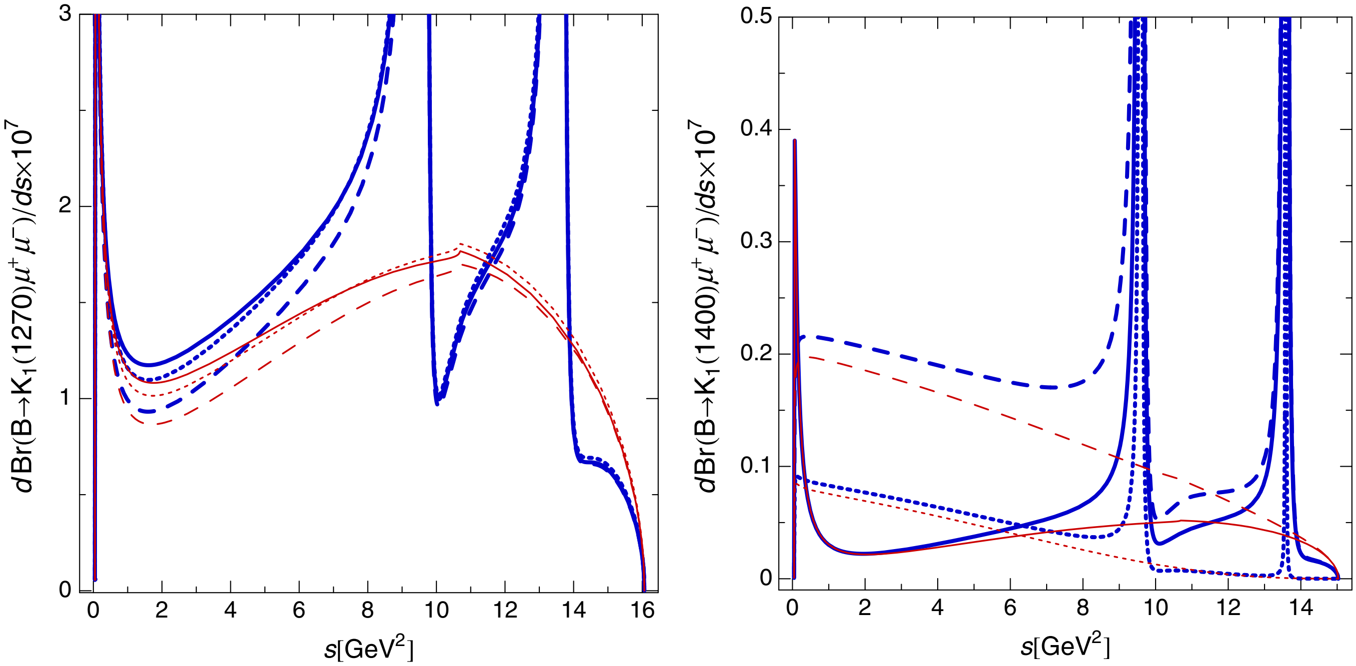

FIG. 1 (color online). The dilepton invariant mass distributions for differential decay rates $d\mathcal{B}(B^- \to K_1^- \mu^+ \mu^-)/ds$ in the SM. The central values of inputs are used. The solid, dotted, and dashed curves correspond to $\theta_{K_1} = -34°, -45°, -57°$, respectively. The thick (blue) [thin (red)] curves correspond to values with [without] resonant corrections.

factors. When the magnitude of θ_{K_1} is increased, this ratio peaks at about $s = 1.5$ GeV^2 (for $\theta_{K_1} \gtrsim 40°$).

B. Branching fractions

In Table VI, we summarize the predictions for branching fractions corresponding to $\theta_{K_1} = -(34 \pm 13)°$. The branching fractions for $B \to K_1 e^+ e^-$ and $B \to K_1 \mu^+ \mu^-$ are close to $B \to K^*(892) e^+ e^-$, $B \to K^*(892) \mu^+ \mu^-$ given in [15]. On the other hand, the branching fractions for $B \to K_1 \tau^+ \tau^-$ decays are very small since the allowed phase space is quite narrow. In Fig. 3, we plot the non-resonant branching fractions $\mathcal{B}_{\rm nr}(B^- \to K_1^- \ell^+ \ell^-)$ as functions of θ_{K_1}. For the range of $\theta_{K_1} = -(34 \pm 13)°$, we obtain $\mathcal{B}_{\rm nr}(B \to K_1(1270)\ell^+\ell^-) \gg \mathcal{B}_{\rm nr}(B \to K_1(1400)\ell^+\ell^-)$. It should be helpful to define the ratio,

$$R_{\ell,{\rm nr}} \equiv \frac{\mathcal{B}_{\rm nr}(B \to K_1(1400)\ell^+\ell^-)}{\mathcal{B}_{\rm nr}(B \to K_1(1270)\ell^+\ell^-)}. \tag{39}$$

We show $R_{\ell,{\rm nr}}$ as functions of the θ_{K_1} in Fig. 4. These ratios sensitively depend on θ_{K_1}, and are smaller than 0.15 for $-47° \le \theta_{K_1} \le -21°$. We predict

$$R_{e,{\rm nr}} = 0.04^{+0.01+0.11}_{-0.01-0.02}, \qquad R_{\mu,{\rm nr}} = 0.03^{+0.01+0.09}_{-0.01-0.01}, \qquad R_{\tau,{\rm nr}} = 0.02^{+0.01+0.07}_{-0.00-0.02}, \tag{40}$$

where the first and second errors correspond to the uncertainties of the form factors and θ_{K_1}, respectively. In Fig. 6, we will further show that the ratio $R_{\mu,{\rm nr}}$ is highly insensitive to the NP corrections.

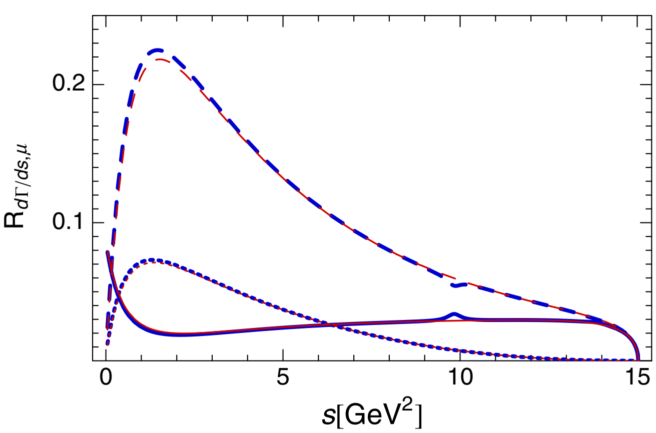

FIG. 2 (color online). The ratio of the decay distributions, $R_{d\Gamma/ds,\mu}$ (see the text), as a function of the dimuon invariant mass s. The legends are the same as in Fig. 1.

C. Forward-backward asymmetry

The differential forward-backward asymmetry of the $\bar{B} \to \bar{K}_1 \ell^+ \ell^-$ decay is defined by

$$\frac{dA_{\rm FB}}{d\hat{s}} \equiv \int_0^{\hat{u}(\hat{s})} d\hat{u} \frac{d^2\Gamma}{d\hat{u} d\hat{s}} - \int_{-\hat{u}(\hat{s})}^0 d\hat{u} \frac{d^2\Gamma}{d\hat{u} d\hat{s}}, \tag{41}$$

which can be written in terms of the quantities in Eqs. (29)–(36) as

TABLE VI. Predictions for the nonresonant branching fractions $\mathcal{B}_{\rm nr}(B \to K_1 \ell^+ \ell^-)$. The first and second errors come from the uncertainty of the form factors and of the θ_{K_1} within the allowed region [26], respectively.

Mode	$\mathcal{B}_{\rm nr} \times 10^6$	Mode	$\mathcal{B}_{\rm nr} \times 10^6$
$B^- \to K_1^-(1270) e^+ e^-$	$2.7^{+1.5+0.0}_{-1.2-0.3}$	$\bar{B}^0 \to \bar{K}_1^0(1270) e^+ e^-$	$2.5^{+1.4+0.0}_{-1.1-0.3}$
$B^- \to K_1^-(1270) \mu^+ \mu^-$	$2.3^{+1.3+0.0}_{-1.0-0.2}$	$\bar{B}^0 \to \bar{K}_1^0(1270) \mu^+ \mu^-$	$2.1^{+1.2+0.0}_{-0.9-0.2}$
$B^- \to K_1^-(1270) \tau^+ \tau^-$	$0.08^{+0.04+0.00}_{-0.03-0.01}$	$\bar{B}^0 \to \bar{K}_1^0(1270) \tau^+ \tau^-$	$0.08^{+0.04+0.00}_{-0.03-0.01}$
$B^- \to K_1^-(1400) e^+ e^-$	$0.10^{+0.03+0.25}_{-0.03-0.05}$	$\bar{B}^0 \to \bar{K}_1^0(1400) e^+ e^-$	$0.09^{+0.03+0.23}_{-0.03-0.04}$
$B^- \to K_1^-(1400) \mu^+ \mu^-$	$0.06^{+0.02+0.18}_{-0.01-0.02}$	$\bar{B}^0 \to \bar{K}_1^0(1400) \mu^+ \mu^-$	$0.06^{+0.02+0.18}_{-0.01-0.02}$
$B^- \to K_1^-(1400) \tau^+ \tau^-$	$0.001^{+0.000+0.005}_{-0.000-0.001}$	$\bar{B}^0 \to \bar{K}_1^0(1400) \tau^+ \tau^-$	$0.001^{+0.000+0.005}_{-0.000-0.001}$

$$\frac{dA_{\rm FB}}{d\hat{s}} = -\frac{G_F^2 \alpha_{\rm em}^2 m_B^5}{2^{10}\pi^5} |V_{ts} V_{tb}^*| \hat{s}\, \hat{u}(\hat{s})^2 \{ {\rm Re}(\mathcal{B}^{K_1} \mathcal{E}^{K_1 *}) + {\rm Re}(\mathcal{A}^{K_1} \mathcal{F}^{K_1 *}) \}, \tag{42}$$

and, after including the hard spectator correction [16], are given by

$$\frac{dA_{\rm FB}}{d\hat{s}} = -\frac{G_F^2 \alpha_{\rm em}^2 m_B^5}{2^{8}\pi^5} |V_{ts}^* V_{tb}|^2 \hat{s}\, \hat{u}(\hat{s})^2 \times c_{10}\Big[{\rm Re}(c_9^{\rm eff}(\hat{s})) A^{K_1} V_1^{K_1} + \frac{\hat{m}_b}{\hat{s}} c_7^{\rm eff} \{ A^{K_1} T_2^{K_1} (1 - \hat{m}_{K_1}) + V_1^{K_1} T_1^{K_1} (1 + \hat{m}_{K_1}) \} + \frac{\hat{m}_b}{\hat{s}} \Delta_{\rm HS} \Big], \tag{43}$$

where $\Delta_{\rm HS}$ is the hard spectator correction given by

$$\Delta_{\rm HS} = \{ (1 + \hat{m}_{K_1}) V_1^{K_1} + (1 - \hat{m}_{K_1})(1 - \hat{s}) A^{K_1} \} \frac{\alpha_s(\mu_h) C_F}{4\pi} \times \frac{\pi^2}{N_c} \frac{f_B f_{K_1}^\perp}{\lambda_{B,+} m_B} \int_0^1 du \Phi_{K_1}^\perp(u) T_{\perp,+}^{(\rm nf)}(u). \tag{44}$$

Here $f_{K_1}^\perp$ and $\Phi_{K_1}^\perp(u)$ are the transverse decay constant and the twist-two tensor light-cone distribution amplitude of the K_1, respectively. $f_{K_1(1270)}^\perp$, $f_{K_1(1400)}^\perp$ and $\Phi_{K_1(1270)}^\perp$, $\Phi_{K_1(1400)}^\perp$ are related with $f_{K_{1A}}^\perp, f_{K_{1B}}^\perp$ and $\Phi_{K_{1A}}^\perp, \Phi_{K_{1B}}^\perp$ by [35]

$$\begin{pmatrix} f_{K_1(1270)}^\perp \\ f_{K_1(1400)}^\perp \end{pmatrix} = M \cdot \begin{pmatrix} f_{K_{1A}}^\perp a_0^{K_{1A},\perp} \\ f_{K_{1B}}^\perp \end{pmatrix}, \tag{45}$$

$$\begin{pmatrix} f_{K_1(1270)}^\perp \Phi_{K_1(1270)}^\perp \\ f_{K_1(1400)}^\perp \Phi_{K_1(1400)}^\perp \end{pmatrix} = M \cdot \begin{pmatrix} f_{K_{1A}}^\perp \Phi_{K_{1A}}^\perp \\ f_{K_{1B}}^\perp \Phi_{K_{1B}}^\perp \end{pmatrix}, \tag{46}$$

where $\Phi_{K_{1A}}^\perp$ and $\Phi_{K_{1B}}^\perp$ are expanded as

$$\Phi_{K_{1A}}^\perp(u) = 6u\bar{u}\Big[a_0^{K_{1A},\perp} + 3a_1^{K_{1B},\perp}\xi + a_2^{K_{1B},\perp}\tfrac{3}{2}(5\xi^2 - 1) \Big], \tag{47}$$

$$\Phi_{K_{1B}}^\perp(u) = 6u\bar{u}\Big[1 + 3a_1^{K_{1B},\perp}\xi + a_2^{K_{1B},\perp}\tfrac{3}{2}(5\xi^2 - 1) \Big], \tag{48}$$

with $a_0^{K_{1B},\perp} \equiv 1$, $\bar{u} \equiv 1 - u$, and $\xi \equiv u - \bar{u}$. The values of $f_{K_{1A}}^\perp$, $f_{K_{1B}}^\perp$ and the Gegenbauer moments, $a_i^{K_1,\perp}$, are tabulated in Table V.

In the following, to compare the theoretical predictions with the data, we use the normalized differential forward-backward asymmetry as

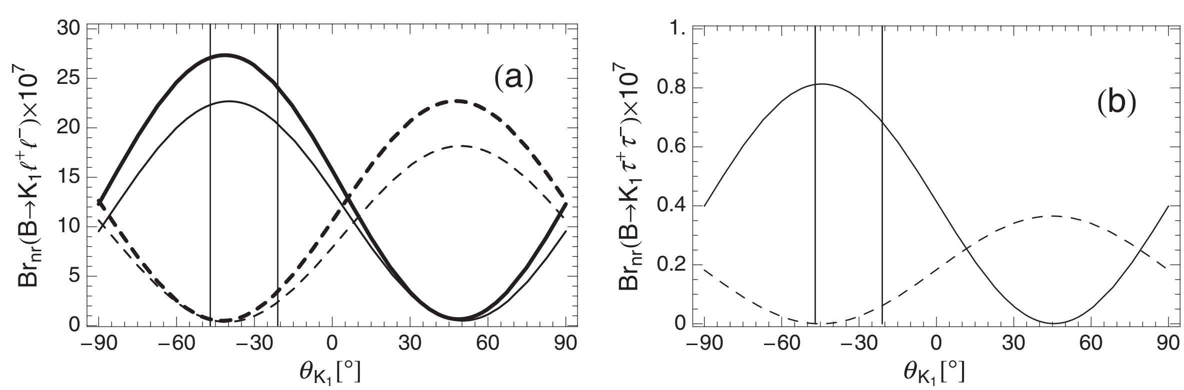

FIG. 3. Nonresonant branching fractions $\mathcal{B}_{\rm nr}(B^- \to K_1^- \ell^+ \ell^-)$ as functions of θ_{K_1}. (a) The thick solid, thick dashed, thin solid, and thin dashed curves correspond to the decays $B \to K_1(1270) e^+ e^-$, $K_1(1400) e^+ e^-$, $K_1(1270) \mu^+ \mu^-$, and $K_1(1400) \mu^+ \mu^-$, respectively. (b) The solid and dashed curves correspond to $B \to K_1(1270) \tau^+ \tau^-$, $B \to K_1(1400) \tau^+ \tau^-$, respectively. The vertical lines indicate the allowed range of θ_{K_1} given in Eq. (2) [26].

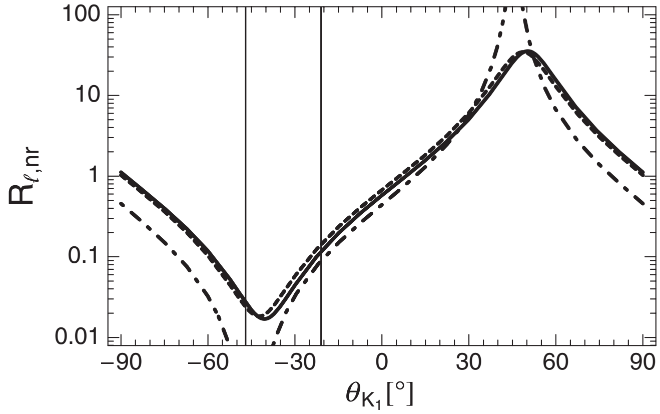

FIG. 4. $R_{\ell,\mathrm{nr}} \equiv \mathcal{B}_{\mathrm{nr}}(B \to K_1(1400)\ell^+\ell^-)/\mathcal{B}_{\mathrm{nr}}(B \to K_1(1270)\ell^+\ell^-)$ as functions of θ_{K_1}. The solid, dashed, and dot-dashed curves correspond to $R_{e,\mathrm{nr}}$, $R_{\mu,\mathrm{nr}}$, and $R_{\tau,\mathrm{nr}}$, respectively. The allowed range of θ_{K_1} given in Eq. (2) [26] is also shown.

$$\frac{d\bar{A}_{\mathrm{FB}}}{d\hat{s}} \equiv \frac{dA_{\mathrm{FB}}}{d\hat{s}} \Big/ \frac{d\Gamma}{d\hat{s}}. \tag{49}$$

In Fig. 5, the normalized differential forward-backward asymmetries $d\bar{A}_{\mathrm{FB}}(B^- \to K_1^- \mu^+\mu^-)/ds$ versus s are plotted. For $B \to K_1(1270)\mu^+\mu^-$ decays, the dependence of $d\bar{A}_{\mathrm{FB}}/ds$ on θ_{K_1} is negligibly small. For $\theta_{K_1} \lesssim -45°$, $d\bar{A}_{\mathrm{FB}}(B \to K_1(1400)\mu^+\mu^-)/ds$ almost vanishes in the region below the J/ψ resonance. We define $s_0^{K_1}$ to be the position of zero of the FBA. $s_0^{K_1}$ satisfies

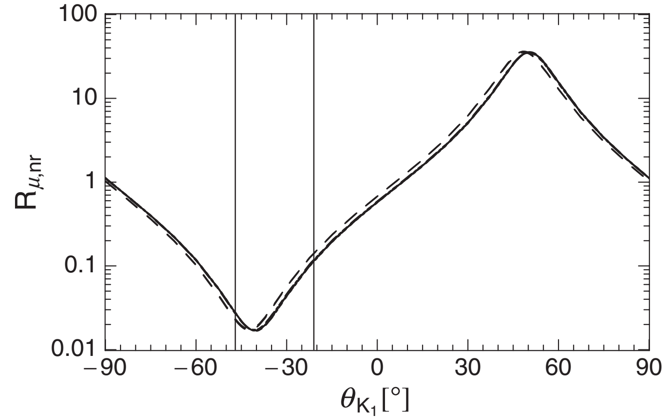

FIG. 6. $R_{\mu,\mathrm{nr}} = \mathcal{B}_{\mathrm{nr}}(B \to K_1(1400)\mu^+\mu^-)/\mathcal{B}_{\mathrm{nr}}(B \to K_1(1270)\mu^+\mu^-)$ as a function of θ_{K_1}. Variations of NP with $(R_7, R_9, R_{10}) = (r, 1, 1)$, $(1, r, 1)$, and $(1, 1, r)$ are, respectively, included, where $r = 1.0$ (solid curve), 1.2 (dotted curve, 0.8 (dot-dashed curve), and -1.0 (dashed curve). The vertical lines indicate the allowed range of θ_{K_1} given in Eq. (2) [26].

$$\frac{\mathrm{Re}(c_9^{\mathrm{eff}}(\hat{s}_0^{K_1}))}{c_7^{\mathrm{eff,HS}}(\hat{s}_0^{K_1})} = -\frac{\hat{m}_b}{\hat{s}_0^{K_1}}\bigg\{\frac{T_2^{K_1}(\hat{s}_0^{K_1})}{V_1^{K_1}(\hat{s}_0^{K_1})}(1-\hat{m}_{K_1}) + \frac{T_1^{K_1}(\hat{s}_0^{K_1})}{A^{K_1}(\hat{s}_0^{K_1})}(1+\hat{m}_{K_1})\bigg\}, \tag{50}$$

which is negative. Here

$$c_7^{\mathrm{eff,HS}}(\hat{s}) \equiv c_7^{\mathrm{eff}} + \frac{\Delta_{\mathrm{HS}}(\hat{s})}{A^{K_1}(\hat{s})T_2^{K_1}(\hat{s})(1-\hat{m}_{K_1}) + V_1^{K_1}(\hat{s})T_1^{K_1}(\hat{s})(1+\hat{m}_{K_1})}. \tag{51}$$

The position of zero appears below the J/ψ-resonance region and depends weakly on θ_{K_1}, especially for $B \to K_1(1270)\ell^+\ell^-$ as shown in Fig. 5. We obtain the positions of the zeros of forward-backward asymmetries to be

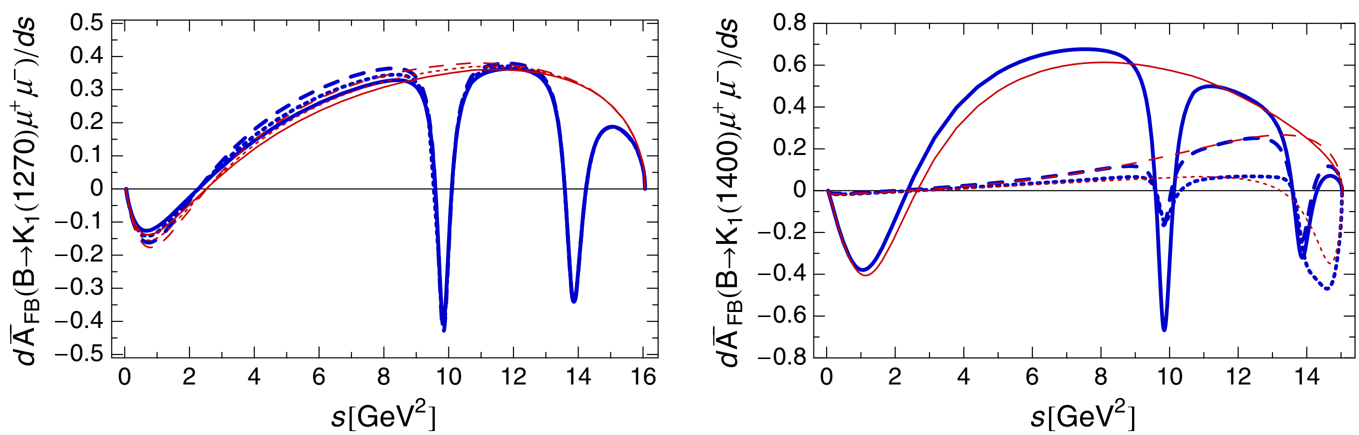

FIG. 5 (color online). Normalized differential forward-backward asymmetries: (a) $d\bar{A}_{\mathrm{FB}}(B^- \to K_1^-(1270)\mu^+\mu^-)/ds$ and (b) $d\bar{A}_{\mathrm{FB}}(B^- \to K_1^-(1400)\mu^+\mu^-)/ds$. The legends are the same as Fig. 1.

$$s_0^{K_1(1270)} = 2.27^{+0.04+0.01}_{-0.07-0.01}\ \text{GeV}^2 \quad \text{and}$$
$$s_0^{K_1(1400)} = 2.80^{+0.23+0.74}_{-0.29-0.07}\ \text{GeV}^2, \tag{52}$$

where the first and second errors correspond to the uncertainties of the form factors and $\theta_{K_1}(= -(34 \pm 13)°)$, respectively. In the following section, we will show that, as the $B \to K^*(892)\ell^+\ell^-$ decay, for the $B \to K_1(1270)\ell^+\ell^-$ decay the position of the zero of the FBA can be a good observable for searching for new-physics effects.

V. NP EFFECTS

In this section, we study the NP corrections to the $B^- \to K_1^- \mu^+ \mu^-$ decays in the model-independent way. As in Ref. [15], we parametrize the NP contributions to the Wilson coefficients as

$$c_i \equiv c_i^{\text{SM}} + c_i^{\text{NP}} = R_i c_i^{\text{SM}} \quad \text{for } c_i = c_7^{\text{eff}}, c_9, c_{10}, \tag{53}$$

at the scale $\bar{m}_b(\bar{m}_b)$. For simplicity, we assume all R_i are real. The model-independent analysis for $B \to X_s \gamma$ and $B \to X_s \ell^+ \ell^-$ [17] gives the following constraints,

$$0.8 \lesssim |R_7| \lesssim 1.2, \qquad 1 \lesssim R_9^2 + R_{10}^2 \lesssim 4. \tag{54}$$

The possibility of a flipped sign of c_7^{eff} due to the NP contribution in the minimum supersymmetric standard model with the minimal flavor violation ansatz and with large $\tan\beta$ has been studied in Ref. [18]. The two-fold constraint was given by

$$-0.02 \le c_7^{\text{NP}} \le 0.12 \quad \text{or} \quad 0.59 \le c_7^{\text{NP}} \le 1.24, \tag{55}$$

at the weak scale. Further constraints on c_7^{NP} have been obtained with

$$c_7^{\text{NP}} = -0.039 \pm 0.043 \cup 0.931 \pm 0.016 \qquad (68\%\text{CL}) \tag{56}$$

$$= [-0.104, 0.026] \cup [0.874, 0.988] \qquad (95\%\text{CL}) \tag{57}$$

in Ref. [37] and

$$c_7^{\text{NP}} = 0.02 \pm 0.047 \cup 0.958 \pm 0.002 \qquad (68\%\text{CL}) \tag{58}$$

$$= [-0.039, 0.08] \cup [0.859, 1.031] \qquad (95\%\text{CL}) \tag{59}$$

in Ref. [38]. The sign of $\text{Re}(c_7^{\text{eff}})$ can also be flipped in

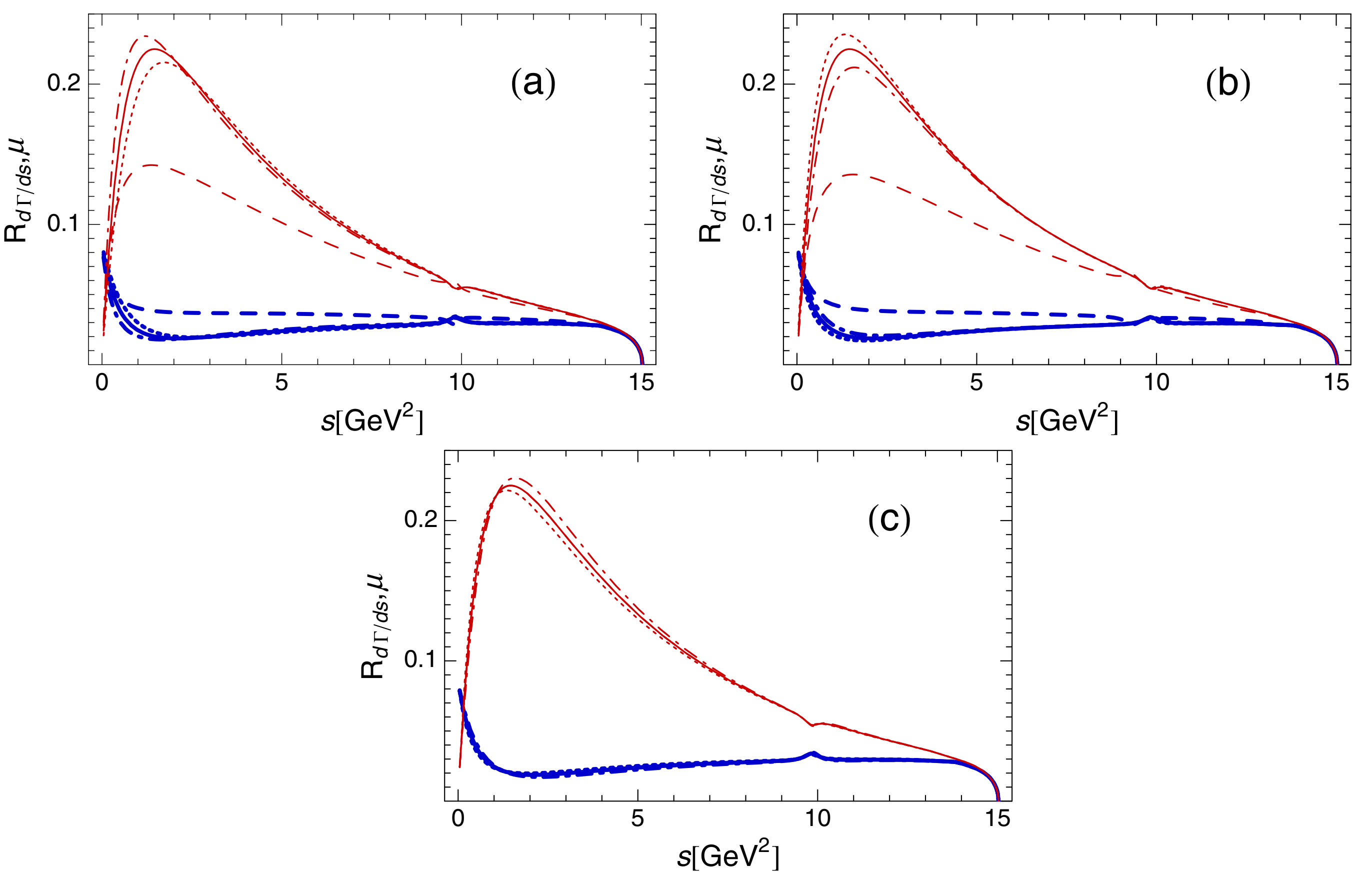

FIG. 7 (color online). $R_{d\Gamma/ds,\mu}$, the ratio of the differential decay rates, as a function of the dimuon invariant mass, s. Variations of R_7, R_9, and R_{10} are depicted in (a), (b), and (c), respectively, where the remaining R_i are set to their SM values. The thick (blue) and thin (red) curves correspond to $\theta_{K_1} = -34°$ and $-57°$, respectively. The solid, dotted, dot-dashed, and dashed curves correspond to $R_i = 1.0$, 1.2, 0.8, and -1.0, respectively.

supersymmetric models with nonminimal flavor violation via gluino-down-squark loops. Furthermore, in general flavor-violating supersymmetric models the sign of c_9 and c_{10} can be flipped. Therefore, in the present paper, we consider $R_i = 1.2$ (i.e. 20% enhancement for the SM Wilson coefficients due to the NP correction), 1.0 (i.e. without the NP correction), 0.8 (i.e. 20% smaller than the SM Wilson coefficients), and -1.0 (i.e. the Wilson coefficients are in opposite signs but have the same magnitudes compared to the SM results).

In Fig. 6, the ratio of the nonresonant branching fractions $R_{\mu,\mathrm{nr}} \equiv \mathcal{B}_{\mathrm{nr}}(B \to K_1(1400)\mu^+\mu^-)/\mathcal{B}_{\mathrm{nr}}(B \to K_1(1270)\mu^+\mu^-)$, including the NP corrections, as a function of the value of θ_{K_1} is depicted. We show that $R_{\mu,\mathrm{nr}}$ is highly insensitive to the NP effect and thus is suitable for determining the value of θ_{K_1}. In Fig. 7, we plot $R_{d\Gamma/ds,\mu}$, the ratio of the differential decay rates, as a function of the dimuon invariant mass, s, where the NP effects are considered. We find that $R_{d\Gamma/ds,\mu}$ is insensitive to variation of R_{10}, whereas its value is increased (decreased) by about 100% (40%) at about $s = 1.5$ GeV^2 corresponding to $\theta_{K_1} = -34°$ $(-57°)$ when R_7 or R_9 equals to -1.

Taking into account the possible NP corrections, we plot $d\bar{A}_{\mathrm{FB}}(B^- \to K_1^-(1270)\mu^+\mu^-)/ds$ as a function of s in Fig. 8. We do not consider the $B^- \to K_1^-(1400)\mu^+\mu^-$ decay, since its branching fraction is relatively small. As shown in Fig. 5 (see also Fig. 8), the differential forward-backward asymmetry for $B \to K_1(1270)\mu^+\mu^-$ and its $s_0^{K_1(1270)}$ (if existing) are very insensitive to the variation of θ_{K_1}. For the cases with c_7^{eff}, c_9, and c_{10} of SM-like sign, the change of the FBA zero owing to variation of NP parameters could be manifest as compared to the hadronic uncertainties. As is well known in the case of $B \to K^*(892)\ell^+\ell^-$, for the flipped sign of c_7^{eff}, c_9, or c_{10} the characteristic features of the FBA change dramatically. Because the asymmetry zero exists only for $\mathrm{Re}(c_9^{\mathrm{eff}})/c_7^{\mathrm{eff}} < 0$ [see Eq. (50)], therefore there is no asymmetry zero for $(R_7, R_9) = (\pm 1, \mp 1)$ in the spectrum. Flipping the sign of

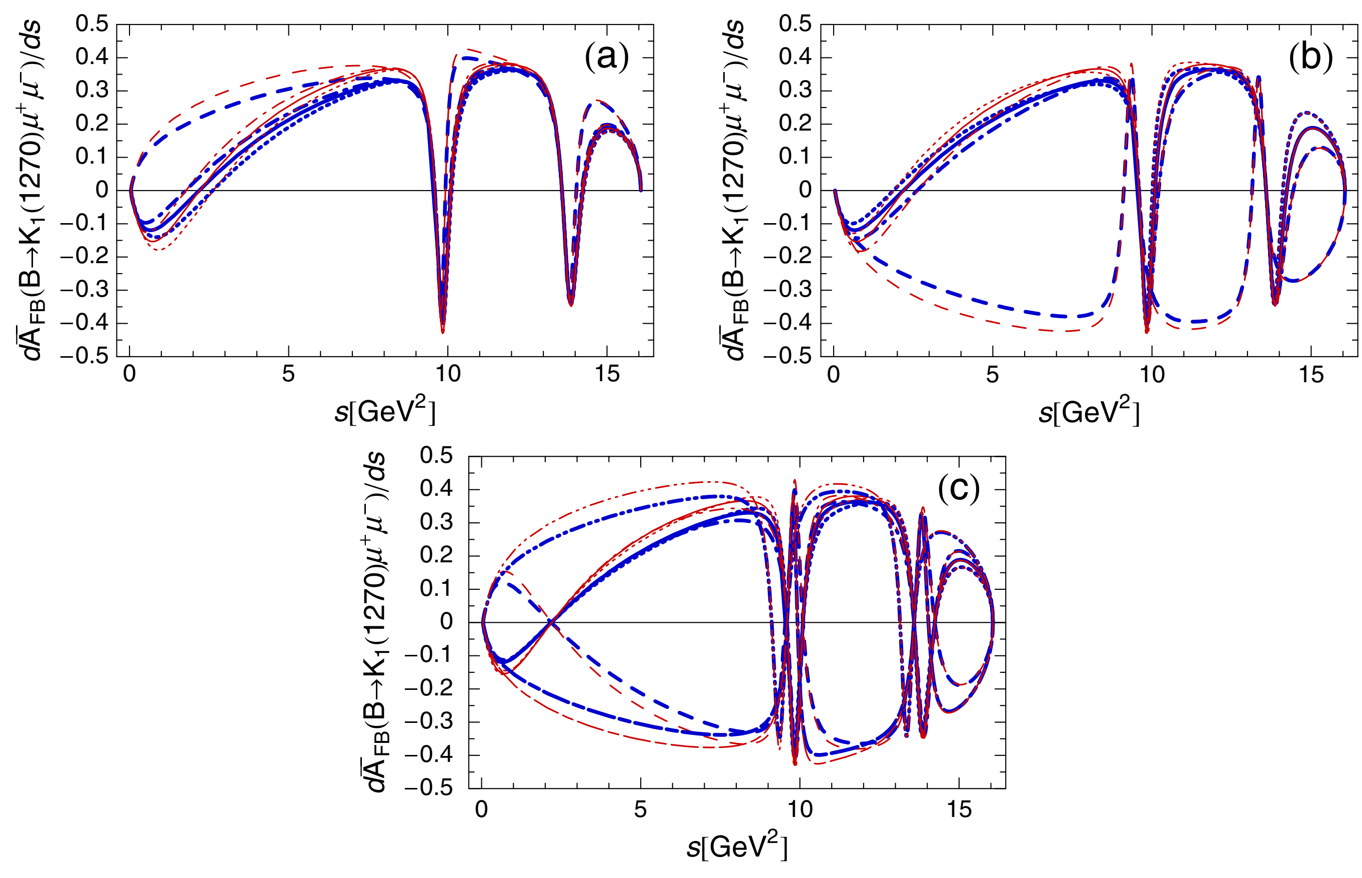

FIG. 8 (color online). Normalized differential forward-backward asymmetry $d\bar{A}_{\mathrm{FB}}(B^- \to K_1^-(1270)\mu^+\mu^-)/ds$ as a function of the dimuon invariant mass s. The thick (blue) and thin (red) curves correspond to the asymmetries with $\theta_{K_1} = -34°$ and $-57°$, respectively. In (a), where $R_9 = R_{10} = 1.0$ (the SM result), the solid curves are for $R_7 = 1.0$, the dotted curves for $R_7 = 1.2$, the dot-dashed curves for $R_7 = 0.8$, and the dashed curves for $R_7 = -1.0$. In (b), where $R_7 = R_{10} = 1.0$ (the SM result), and the solid curves are for $R_9 = 1.0$, the dotted curves for $R_9 = 1.2$, the dot-dashed curves for $R_9 = 0.8$, and the dashed curves for $R_9 = -1.0$. In (c), where $R_7 = R_9 = 1.0$ and the solid curves are for $R_{10} = 1.0$ (the SM result), the dotted curves for $R_{10} = 1.2$, the dot-dashed curves for $R_{10} = 0.8$, and the dashed curves for $R_{10} = -1.0$. The $d\bar{A}_{\mathrm{FB}}/ds$ with $(R_7, R_9, R_{10}) = (1.0, -1.0, -1.0)$, and $(-1.0, 1.0, -1.0)$ are denoted by the double-dot-dashed and long-short dashed curves, respectively, in (c).

c_{10} would change the sign of the FBA. From the above discussions we can conclude that the position of the FBA zero for the $B \to K_1(1270)\ell^+\ell^-$ decay is a suitable quantity to constrain the NP parameters. Recent measurements for $B \to K^*(892)\ell^+\ell^-$ decays [8,9] seem to favor (i) the flipped sign of c_7^{eff} which is denoted by the dashed curves in Fig. 8(a), or (ii) the simultaneous flip of the sign of c_9 and c_{10} which are denoted by the double-dot-dashed curves in Fig. 8(c). However, they disfavor the flipped sign$(c_9 c_{10})$ models. See also the discussion in Ref. [20].

VI. SUMMARY

We have studied the rare decays $B \to K_1\ell^+\ell^-$ with $K_1 \equiv K_1(1270)$, $K_1(1400)$ and $\ell \equiv e, \mu, \tau$. The strange axial-vector mesons, $K_1(1270)$ and $K_1(1400)$, are the mixtures of the K_{1A} and K_{1B}, which are the 1^3P_1 and 1^1P_1 states, respectively. Although the branching ratios depend on the magnitudes of $B \to K_1$ form factors, the $K_1(1270) - K_1(1400)$ mixing angle, θ_{K_1}, can be well determined from the measurement of the ratio $R_\ell \equiv \mathcal{B}(B \to K_1(1400)\ell^+\ell^-)/\mathcal{B}(B \to K_1(1270)\ell^+\ell^-)$, which depends very weakly on new-physics corrections. We have calculated differential forward-backward asymmetries of $B \to K_1\mu^+\mu^-$ decays. For $B \to K_1(1270)\mu^+\mu^-$, the asymmetry zero, which depends very weakly on θ_{K_1}, can be dramatically changed due to variation of new-physics parameters.

ACKNOWLEDGMENTS

This research was supported in part by the National Science Council of the Republic of China under Grants No. NSC96-2112-M-033-004-MY3 and No. NSC96-2811-M-033-004.

[1] E. Barberio *et al.*, arXiv:0808.1297.
[2] B. Aubert *et al.* (*BABAR* Collaboration), Phys. Rev. D **70**, 112006 (2004).
[3] M. Nakao *et al.* (Belle Collaboration), Phys. Rev. D **69**, 112001 (2004).
[4] T. E. Coan *et al.* (CLEO Collaboration), Phys. Rev. Lett. **84**, 5283 (2000).
[5] H. Yang *et al.*, Phys. Rev. Lett. **94**, 111802 (2005).
[6] A. Ishikawa *et al.* (Belle Collaboration), Phys. Rev. Lett. **91**, 261601 (2003).
[7] B. Aubert *et al.* (*BABAR* Collaboration), Phys. Rev. D **73**, 092001 (2006).
[8] A. Ishikawa *et al.* (Belle Collaboration), Phys. Rev. Lett. **96**, 251801 (2006).
[9] B. Aubert *et al.* (*BABAR* Collaboration), arXiv:0804.4412.
[10] B. Aubert *et al.* (*BABAR* Collaboration), arXiv:0807.4119.
[11] G. Eigen, arXiv:0807.4076.
[12] M. A. Paracha, I. Ahmed, and M. J. Aslam, Eur. Phys. J. C **52**, 967 (2007).
[13] I. Ahmed, M. A. Paracha, and M. J. Aslam, Eur. Phys. J. C **54**, 591 (2008).
[14] A. Saddique, M. J. Aslam, and C. D. Lu, Eur. Phys. J. C **56**, 267 (2008).
[15] A. Ali, P. Ball, L. T. Handoko, and G. Hiller, Phys. Rev. D **61**, 074024 (2000).
[16] M. Beneke, T. Feldmann, and D. Seidel, Nucl. Phys. **B612**, 25 (2001).
[17] A. Ali, E. Lunghi, C. Greub, and G. Hiller, Phys. Rev. D **66**, 034002 (2002).
[18] T. Feldmann and J. Matias, J. High Energy Phys. 01 (2003) 074.
[19] F. Kruger and J. Matias, Phys. Rev. D **71**, 094009 (2005).
[20] C. Bobeth, G. Hiller, and G. Piranishvili, J. High Energy Phys. 07 (2008) 106.
[21] U. Egede, T. Hurth, J. Matias, M. Ramon, and W. Reece, arXiv:0807.2589.
[22] C. H. Chen, C. Q. Geng, and L. Li, arXiv:0808.0127.
[23] M. Suzuki, Phys. Rev. D **47**, 1252 (1993).
[24] L. Burakovsky and J. T. Goldman, Phys. Rev. D **57**, 2879 (1998).
[25] H. Y. Cheng, Phys. Rev. D **67**, 094007 (2003).
[26] H. Hatanaka and K. C. Yang, Phys. Rev. D **77**, 094023 (2008).
[27] A. J. Buras, M. Misiak, M. Munz, and S. Pokorski, Nucl. Phys. **B424**, 374 (1994).
[28] A. J. Buras and M. Munz, Phys. Rev. D **52**, 186 (1995).
[29] C. S. Lim, T. Morozumi, and A. I. Sanda, Phys. Lett. B **218**, 343 (1989).
[30] A. Ali, T. Mannel, and T. Morozumi, Phys. Lett. B **273**, 505 (1991).
[31] F. Kruger and L. M. Sehgal, Phys. Lett. B **380**, 199 (1996).
[32] W. M. Yao *et al.* (Particle Data Group), J. Phys. G **33**, 1 (2006).
[33] K. C. Yang, Phys. Rev. D **78**, 034018 (2008).
[34] K. C. Yang (unpublished).
[35] K. C. Yang, Nucl. Phys. **B776**, 187 (2007).
[36] CKM fitter group, http://ckmfitter.in2p3.fr.
[37] U. Haisch and A. Weiler, Phys. Rev. D **76**, 074027 (2007).
[38] C. Bobeth, M. Bona, A. J. Buras, T. Ewerth, M. Pierini, L. Silvestrini, and A. Weiler, Nucl. Phys. **B726**, 252 (2005).